

Removal of Pb(II) in Aqueous Solutions Using Synthesized Zeolite X from Ecuadorian Clay

Remoción de Pb(II) en soluciones acuosas usando zeolita X sintetizada a partir de arcilla ecuatoriana

Daniel F. Medina-Rodríguez¹, Delly M. San Martín-Torres², Carmen M. López de García³, Luis V. García-Berfon⁴, Silvio D. Aguilar-Ramírez⁵, Ximena V. Jaramillo-Fierro⁶, Daniel J. Rosado-Alcarria⁷, and Adriana L. García-López⁸

ABSTRACT

Zeolite X was synthesized from clay using the alkaline fusion method and hydrothermal treatment to remove Pb(II) in aqueous solutions. Clay and zeolite were characterized through X-ray diffraction and fluorescence (XRD, FRX), as well as through specific surface area (SSA). The adsorbents were prepared as cylindrical extrudates using clay and a clay-zeolite combination (60-40%, respectively). The effects of pH, isotherm, and adsorption kinetics on the removal of Pb(II) in solutions of 80 mg Pb(II)/L were studied. It was possible to obtain a zeolite X from clay, with an SSA of 376 m²/g, 30 times greater than that of clay (12 m²/g). In the combined extrudate was present the zeolitic structure, with an SSA 12 times higher compared to the clay extrudate. The adsorption capacity, at 30 °C and V/m ratio of 1 g/L, is almost double compared to the clay extrudate (24 mg Pb(II)/g vs. 13 mg Pb(II)/g). Adsorption follows second order kinetics, and the Langmuir isotherm equation showed a good fit with the experimental equilibrium data for the two extrudates. The Webber-Morris and Bangham-Burt's models suggest that pore and film diffusion influence the kinetic mechanism.

Keywords: Pb(II) removal, heavy metals, alkaline fusion, zeolite synthesis

RESUMEN

Se sintetizó zeolita X a partir de arcilla utilizando el método de fusión alcalina y tratamiento hidrotérmico para eliminar Pb(II) en soluciones acuosas. La arcilla y la zeolita se caracterizaron por difracción y fluorescencia de rayos X (XRD, FRX), así como por área específica (SSA). Los adsorbentes se prepararon como extruidos cilíndricos usando arcilla y una combinación de arcilla-zeolita (60-40%, respectivamente). Se estudiaron los efectos del pH, la isoterma y cinética de adsorción en la remoción de Pb(II) en soluciones de 80 mg Pb(II)/L. Fue posible obtener zeolita X a partir de la arcilla, con una SSA de 376 m²/g, 30 veces mayor que la de arcilla (12 m²/g). En el extrudado combinado estuvo presente la estructura zeolítica, con una SSA 12 veces mayor comparado con el extruido de arcilla. La capacidad de adsorción, a 30 °C y relación V/m de 1 g/L, es casi el doble comparada con el extruido de arcilla (24 mg Pb(II)/g frente a 13 mg de Pb(II)/g). La adsorción sigue la cinética de segundo orden, y la ecuación de isoterma de Langmuir mostró un buen ajuste con los datos experimentales de equilibrio para los dos extruidos. Los modelos de Webber-Morris y Bangham-Burt sugieren que la difusión en la película y en los poros influye en el mecanismo cinético.

Palabras clave: remoción de Pb(II), metales pesados, fusión alcalina, síntesis de zeolita

Received: August 3rd, 2020

Accepted: February 18th, 2021

¹Daniel Fernando Medina. Master in Applied Chemistry from the Universidad Técnica Particular de Loja. Affiliation: Universidad Técnica Particular de Loja, Ecuador. Email: dfmedina4@utpl.edu.ec

²Delly Maribel San Martín. Master in Applied Chemistry from the Universidad Técnica Particular de Loja. Affiliation: Universidad Técnica Particular de Loja, Ecuador. Email: maribel22sanmartin@gmail.com

³Carmen Milena López. Doctor of Science, Major in Chemistry from Universidad Central de Venezuela. Affiliation: Universidad Técnica Particular de Loja, Ecuador. Email: milena.lopez2009@gmail.com

⁴Luis Vicente García. Doctor of Science, Major in Chemistry from Universidad Central de Venezuela. Affiliation: Universidad Técnica Particular de Loja, Ecuador. Email: lvgarcia4@utpl.edu.ec

⁵Silvio David Aguilar. Master in Applied Chemistry from the Universidad Técnica Particular de Loja. Affiliation: Universidad Técnica Particular de Loja, Ecuador. Email: sdaguilar@utpl.edu.ec

⁶Ximena Verónica Jaramillo. Master in Applied Chemistry from the Universidad Técnica Particular de Loja. Affiliation: Universidad Técnica Particular de Loja, Ecuador. Email: xvjaramillo@utpl.edu.ec

⁷Daniel Jesús Rosado. Doctor in Chemical and Environmental Technology from Universidad de Sevilla (Spain). Affiliation: University of Kiel, Germany. Email: drosado@hydrology.uni-kiel.de

Introduction

Lead (Pb) is a natural element of the Earth's crust present in the air, water, and soil. Due to its unique characteristics, humans have used lead in different manufactured products that have become its main anthropogenic sources, such as leaded gasoline, paints, ceramics, solders, water tanks, hair

⁸Adriana Lucía García. Doctor of Engineering Sciences from Universidad Central de Venezuela. Affiliation: Universidad Central de Venezuela, Venezuela. Email: adriana.ucv@gmail.com

How to cite: Medina, D. F., San Martín, D. M., López, C. M., García, L. V., Aguilar, S. D., Jaramillo, X. V., Rosado, D. J., and García, A. L. (2021). Removal of Pb(II) In Aqueous Solutions using Synthesized Zeolite X from Ecuadorian Clay. *Ingeniería e Investigación*, 41(2), e89671. [10.15446/ing.investig.v41n2.89671](https://doi.org/10.15446/ing.investig.v41n2.89671)



Attribution 4.0 International (CC BY 4.0) Share - Adapt

dye, cosmetics, airplanes, agricultural machinery, armour for X-ray machines, etc. (Boskabady *et al.*, 2018). However, lead is also an environmental pollutant and a non-biodegradable toxic metal, with well-known toxic effects (Poma, 2008). Therefore, it poses a risk to public health and, as a result, the world health organization, as well as other international organizations, has established a Pb(II) limit for drinking water of 0,01 mg Pb(II)/L (Uddin, 2017).

To stop releasing of Pb(II) into the environment and improve public health, it is necessary to remove Pb(II) from industrial wastewater. It is common today to use a large number of techniques for this purpose, including ion exchange, reverse osmosis, precipitation, and adsorption (Carolin, Kumar, Saravanan, Joshiba, and Nau-shad, 2017). Adsorption is an efficient separation technique that has been in use for a long time to remove heavy metal ions. In aqueous solutions, a wide variety of solid adsorbents have been reported, such as natural zeolites (Belova, 2019), bentonite (Ramola, Belwal, Li, Wang, and Zhou, 2020), cassava peel (Albis, 2016), activated carbon (Zafarzadeh, Sadeghi, Golbini-Mofrad, and Beirami, 2018), carbon nanotubes (Wang, Zhou, Peng, Yu, and Yang, 2007) or clay monoliths (Ahrouch, Gatica, Draoui, Bellido, and Vidal, 2019), among others.

Zeolites are crystalline solids with pores of molecular dimensions that allow the passage of molecules below a certain size depending on the porous system of the material. Zeolites contain mainly silicon, aluminium, oxygen, and some metals, including titanium, tin, zinc, and others. They have applications in adsorption, catalysis, ion exchange, and biological processes (Montalvo, Huilínir, Borja, Sánchez, and Hermann, 2020).

Clays have been used as a source of silicon and aluminium in zeolite synthesis (Ayele, Pérez-Pariente, Chebude, and Díaz, 2016; Luo, Lau, Wu, Zhu, and Yang, 2018), since they are abundant and cheap materials in many countries, as is the case of Ecuador. Clays are very abundant silicoaluminates worldwide. They are used mainly for to manufacture construction materials such as bricks and tiles, as well as in the ceramic sector (Wi, Yang, Park, Chang, and Kim, 2020; Moussi *et al.*, 2020).

Synthetic zeolites with a faujasite structure (FAU) have been effective for the removal of Pb(II) in wastewater (Pandey, Sharma, and Sambhi, 2015; Shariatnia and Bagherpour, 2018). In light of the above, this research aims to synthesize zeolite from Ecuadorian clay and evaluate its potential as an adsorbent for the removal of Pb(II). In this work, faujasite type X zeolite was synthesized from clay from southern Ecuador, and cylindrical extrudates were prepared to evaluate its performance as an adsorbent in the removal of Pb(II) using an aqueous solution prepared in the laboratory. It was compared the behaviour of extrudates prepared with clay and those prepared with zeolite-clay mixtures.

Methods and materials

Materials and reagents

The starting clay, collected in the province of Loja, Ecuador, was named PACL-029. This clay, available in lumps of relatively large size, was oven-dried at 90 °C overnight, then crushed and sieved to a No. 200 ASTM mesh (0,075 mm) (Gilson Co., n.d).

The following reagents were used:

- Sodium hydroxide in lentils, 98%, Merck, Germany.
- Sodium aluminate (solid), 50-56% Al₂O₃-37-45% Na₂O, Sigma Aldrich, United States.

Zeolite synthesis

In summary, the synthesis conditions were set based on previous work on zeolite synthesis from aluminosilicate gels (García, López, García, Casanova, and Goldwasser, 2016). The composition set for the synthesis mixture was $\frac{SiO_2}{Al_2O_3} = 4$, $\frac{Na_2O}{SiO_2} = 1,65$, and $\frac{H_2O}{Na_2O} = 40$. Since the employed clay has a $\frac{SiO_2}{Al_2O_3}$ ratio equal to eight, it was necessary to add sodium aluminate as an additional aluminium source to decrease the molar $\frac{SiO_2}{Al_2O_3}$ ratio to four.

The detailed process consisted of the following steps:

- Mixing 30 g of clay with 35 g of NaOH dissolved in 50 ml of water to form a homogeneous mud;
- calcinating the clay-NaOH mud at 800 °C for 4 h;
- trituration of the calcined product and mixing with a solution prepared by dissolving 15 g of sodium aluminate in 390 ml of water and stirring the mixture at room temperature for 1 h to homogenize;
- keeping the mixture at room temperature for 24 h (aging);
- a hydrothermal treatment of the mixture in covered and heated containers at 90 °C for 24 h;
- separating the solid product by filtration, washing with water to remove excess alkali, and drying at 90 °C overnight; and
- packaging the solid for subsequent characterization (the zeolitic product obtained with this procedure is the sodic form).

Preparation of adsorbents

For the evaluation of the solids as adsorbents, cylindrical extrudates with approximate dimensions of 0,5 cm in length and 0,25 cm in diameter were prepared. The preparation of these solids consisted of the following stages:

- (i) mixing of the solid materials in zeolite (clay ratio 40:60) adding water (approximately 35%) to form a mixture with good plasticity;
- (ii) extruding the mixture using a syringe with a 2,5 mm diameter plunger (the mixture is expelled at a constant speed, thus achieving extrudate threads with a diameter equal to the opening of the syringe);
- (iii) drying the extrudates at 90 °C for 12 h;
- (iv) Calcining in a muffle furnace with the following heating program: from room temperature to 100 °C at a rate of 2 °C/min, maintaining this temperature for 40 min, and increasing to 550 °C at a rate of 3 °C/min, leaving 550 °C for 8 h.

Characterization of solids

X-Ray diffraction measurements of the clay, synthesized zeolite, and the extrudates were performed on a Bruker model D8 Advanced, equipped with a solid-state LynxEye detector, using Cu K α radiation ($\lambda = 1,5406 \text{ \AA}$), operated at 40 kV and 25 mA, with a step width of 0,02044 in a 2θ range of 4,0-60,0°. The chemical composition was determined through X-Ray Fluorescence (XRF) in a portable Bruker model S1-turbo^{SD}, using the Mining Light Elements measurement method.

The determination of the specific surface area of the solids (m²/g) was carried out in the ChemiSorb 2720 equipment from Micromeritics, by adsorption of nitrogen at the temperature of liquid nitrogen (-196 °C) with a 30% gas mixture of diluted N₂ in He. The Chemisoft TPxV1.03 software allows calculating the specific surface area by applying the BET equation and the single point method (Webb, Orr, Camp, Olivier, and Yunes, 1997). The scanning electron microscopy (SEM) micrographs were taken on a Hitachi S-500 at 20 keV and 50 mA.

Pb(II) removal studies

Effect of pH: With the extrudates prepared with clay and extrudates prepared with zeolite-clay, an experiment was carried out consisting of contacting 25 mg of adsorbent with 25 mL (1g of solid per liter of solution) of 80 mg Pb(II)/L solution at 30 °C for 24 h and 100 rpm. The pH was adjusted to 4,03, 4,97, 6,06 and, 6,99 with 0,1 M HCl or NaOH solutions. The pH interval was chosen based on Pandey's work (Pandey *et al.*, 2015).

Adsorption equilibrium studies: For this study, Pb(II) solutions of 20, 40, 60, 80, 110, 140, 180, and 240 mg/L were used. The solution was maintained at pH = 5 based on the results obtained from the studied pH interval. The extrudates and an amount of Pb(II) solution, with a ratio of 1 g of solid per liter of solution, were placed in an Erlenmeyer flask of 100 mL. The above recipients were placed in an orbital agitator (Thermo Scientific SHKA2000) at 30 °C for 24 h and 100 rpm.

Adsorption isotherm: The adsorption capacity of solids can be determined by analyzing the equilibrium data through

isotherm models. An equilibrium isotherm relates the amount adsorbed and the concentration remaining in the solution in equilibrium. The Langmuir, Freundlich, and Temkin isotherm models were applied in this research (Bhatt *et al.*, 2012).

The Langmuir isotherm assumes a surface with homogeneous adsorption sites, without interactions between adsorbed species. Equation (1) represents the linear form of this isotherm (Bhatt *et al.*, 2012):

$$\frac{C_e}{Q_e} = \frac{1}{Q_m} * C_e + \frac{1}{K_L Q_m} \quad (1)$$

where

Q_e = equilibrium adsorption capacity, mg Pb(II)/g of adsorbent

Q_m = maximum adsorption capacity, mg Pb(II)/g of adsorbent

C_e = equilibrium concentration, mg Pb(II)/g of adsorbent

K_L = Langmuir adsorption constant, L/mg Pb(II)

Plotting $\frac{C_e}{Q_e}$ against C_e obtains a straight line with slope and intercept of $\frac{1}{Q_m}$ and $\frac{1}{K_L Q_m}$ respectively. K_L is a tool to the calculation of the dimensionless equilibrium parameter (R_L) calculated using Equation (2) (Bhatt *et al.*, 2012).

$$R_L = \frac{1}{(1 + K_L C_0)} \quad (2)$$

where

C_0 = initial concentration, mg Pb(II)/g of adsorbent

The Freundlich isotherm is an empirical model that describes monolayer and multilayer adsorption, expressed mathematically as Equation (3) (Bhatt *et al.*, 2012).

$$\log Q_e = \frac{1}{n} \log C_e + \log K_f \quad (3)$$

K_f and n are Freundlich constants incorporating the factors affecting the adsorption capacity and adsorption intensity, respectively. Plotting $\log Q_e$ vs. $\log C_e$ results in a linear graph with slope $\frac{1}{n}$ and intercept $\log K_f$, from which n and K_f can be calculated.

The Temkin isotherm model assumes that the adsorption heat decreases linearly with the increase in coverage of the adsorbent surface and a uniform distribution of binding energies up to a maximum binding energy. Equation (4) describes the Temkin isotherm (Inyibor, Adekola and Olatunyi, 2016):

$$Q_e = B \ln A + B \ln C_e \quad (4)$$

B is a constant related to the heat of adsorption, and A is the Temkin isotherm constant (L/g). From the plot of Q_e vs $\ln C_e$, B and A can be calculated from the slope (B) and intercept ($B \ln A$) (Inyibor, Adekola and Olatunyi, 2016).

In all cases, the equilibrium adsorption capacity, Q_e , was determined through Equation (5) (Bhatt *et al.*, 2012).

$$Q_e = (C_0 - C_e) * \left(\frac{V}{m}\right) \quad (5)$$

$\frac{V}{m}$ is the relationship between the Volume of solution in L (V) and mass of solid in g (m) used in the experiment. In all experiments, the $\frac{V}{m}$ ratio was the unity.

Adsorption kinetics studies: A plot of sorption vs. time usually indicates the adsorption kinetics. For kinetics experiments, the $\left(\frac{V}{m}\right)$ ratio was kept equal to unity: 500 mg of solid in 500 mL of 80 mg Pb(II)/L solution at 100 rpm and 30 °C. The sampling was performed in triplicate from time zero to 180 minutes, taking the average value in each measurement. The adsorption capacity of the solid (q), expressed as mg of Pb(II)/g, was determined through Equation (6) (Tan and Hamed, 2017):

$$q = (C_0 - C) * \left(\frac{V}{m}\right) \quad (6)$$

where q is the adsorption capacity of the solid for any time t , expressed as mg Pb(II)/g extrudate; C_0 and C , represents the metal concentration initial and at time t , respectively. In all of the above experiments, the Pb content in the solutions was determined on a Perkin Elmer Analyst 400 atomic absorption spectrometer.

Adsorption kinetics were investigated using pseudo first order (PFO), pseudo second order (PSO), and Elovich models. The diffusion mechanism was studied applying the Bangham-Burt and Webber-Morris intra-particle diffusion models (Tan and Hamed, 2017).

The pseudo first order (PFO) model has the linear form given in Equation (7) (Tan and Hamed, 2017).

$$\ln(q_e - q) = \ln(q_e) - k_1 t \quad (7)$$

where q_e is the equilibrium adsorption capacity (mg/g) at time t (the process time), k_1 is the pseudo first order rate constant which is calculated from the slope of the plot of $\ln(q_e - q)$ vs. time.

The PSO model assumes that the sorption rate is of the second order with respect to accessible active sites. Equation (8) shows the linear form of this model, where k_2 is the rate constant. A plot of $\frac{t}{q}$ vs. t produces a straight line for conforming kinetics. The values of k_2 and q_e are obtained from the slope and the intercept (Tan and Hamed, 2017).

$$\frac{t}{q} = \frac{1}{k_2 q_e^2} + \frac{t}{q_e} \quad (8)$$

The linear form of the Elovich model is presented in Equation (9), where α is the initial adsorption rate (mg/g.min) and β is the desorption constant associated with surface coverage. Kinetic data obeying this model would produce a straight line from the plot of q vs. $\ln t$. The slope and intercept are equal to $\left(\frac{1}{\beta}\right)$ and $\left(\frac{1}{\beta}\right) \ln(\alpha\beta)$, respectively (Tan and Hamed, 2017).

$$q = \left(\frac{1}{\beta}\right) \ln(\alpha\beta) + \left(\frac{1}{\beta}\right) \ln t \quad (9)$$

Bangham's model is usually applied to verify if pore diffusion is the only rate-controlling mechanism during an adsorptive process. It is generally used in the following form

(Equation 10) (Tan and Hamed, 2017):

$$\lg\left(\log\left(\frac{C_0}{C_0 - q\bar{m}}\right)\right) = \log\left(\frac{k_0 \bar{m}}{2.303 V}\right) + \alpha \log t \quad (10)$$

where V is the volume of the solution (mL), \bar{m} is the amount of extrudate per volume of solution in g/L, and k_0 and α are constants. In order to check the Bangham-Burt model, a plot of $\log\left(\log\left(\frac{C_0}{C_0 - q\left(\frac{V}{m}\right)}\right)\right)$ vs. $\log t$ should produce a straight line.

The Webber-Morris model (Equation 11), is also used to describe adsorption kinetics controlled by intra-particle diffusion (Equation 11), (Tan and Hamed, 2017).

$$q = k_{id} \sqrt{t} + B \quad (11)$$

where k_{id} is the intra-particle diffusion rate constant $\left(\frac{mg}{g \text{ min}^{1/2}}\right)$, while B is the initial adsorption capacity (mg/g). To validate the Webber-Morris model, a plot of q vs. \sqrt{t} should be linear with k_{id} and B obtained as the slope and intercept, respectively.

Results and discussion

Characterization of clay and synthesized zeolite

The XRD pattern of the original clay (Figure 1) indicates the presence of these phases: heulandite (9,80 and 11,11° 2 θ), cristobalite (22 and 36° 2 θ), quartz (26,6° 2 θ), and anorthite (28° 2 θ). The XRD lines of the clay have a low intensity, indicating a low proportion of the identified clay minerals. For the synthesis, the alkaline fusion method recommended by various authors was used to obtain zeolites from clays, porcelain, and ashes (Ayele *et al.*, 2016; Bai, Zha, Chang, Zhang, and Chu, 2018; Kongnoo, Tontisirin, Worathanakul, and Phalakornkule, 2017; Ke, Shen, and Yang, 2019; Boycheva, 2020; Wajima and Ikegami, 2009). It was possible to zeolitize the clay through the applied method, since the synthesis product has the characteristic XRD pattern of the Faujasite structure (Figure 2), without the presence of lines corresponding to other crystalline phases (Treacy and Higgins, 2001). However, it cannot rule out the presence of amorphous phases not detectable by XRD.

The cell parameter a_0 (Å) of the synthesized zeolite was determined from the XRD pattern of the solid (Figure 2) according to the equation of the cubic crystalline system of the FAU structure. This parameter was calculated for each of the XRD lines at positions 15,44, 23,35, 26,70, and 30,92 position 2 θ , Cu, taking the average value of the determinations. The number of structural Al atoms in the zeolite was determined using the Breck-Flanigen equation (Giannetto, Montes, and Rodríguez, 2000), and the structural Si/Al ratio of the synthesized zeolite was calculated with this value. The calculated value for a_0 was 24,99 Å with $\left(\frac{Si}{Al}\right)_{DRX} = 1,08$ (Table 1). These values classify the synthesized zeolite as type X Faujasite (FAU). Therefore, the nomenclature used for this zeolite was FAU-Na.

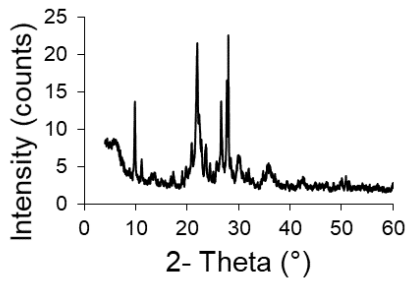


Figure 1. XRD pattern of PACL-029.
Source: Authors

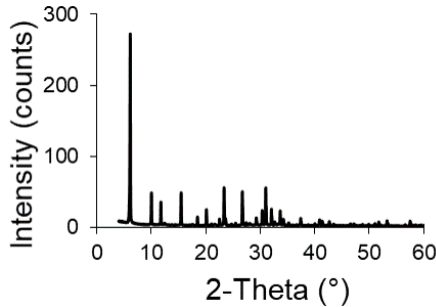


Figure 2. XRD pattern of FAU-Na.
Source: Authors

Figure 3 shows a SEM micrograph of the synthesized FAU-Na zeolite. The sample showed the typical morphology of octahedral crystalline aggregates, whose size aggregates can be lower than 1 μm .

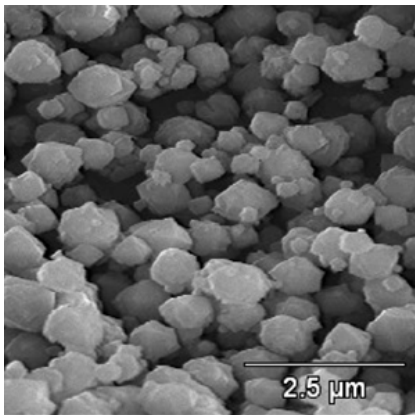


Figure 3. SEM micrograph of the FAU-Na zeolite.
Source: Authors

Table 1 shows the values of mass percentage of SiO_2 and Al_2O_3 , the molar $\left(\frac{\text{SiO}_2}{\text{Al}_2\text{O}_3}\right)$ ratio, and values of specific surface area (SSA) of the synthesized zeolite and clay. The synthesized zeolite has a SSA value 30 times higher than that of clay, due to the structural difference between the two solids. The dense phases that constitute the clay as cristobalite, quartz, and anorthite have low SSA values (about 3 m^2/g) (Bustillo, Fort, and Bustillo, 1993), whereas the synthetic Faujasite zeolite can have SSA values of up to 700 m^2/g (Garcia et al 2016).

The chemical composition also changes with respect to the clay; the molar $\frac{\text{SiO}_2}{\text{Al}_2\text{O}_3}$ ratio in the zeolite is lower because it was changed in the synthesis mixture by the addition of the aluminium source. The determined value of the ratio $\left(\frac{\text{SiO}_2}{\text{Al}_2\text{O}_3}\right)_{\text{FRX molar}}$ in the zeolite was lower than that used in the synthesis mixture, which suggests that soluble silicate species formed during the alkaline fusion process remain in the synthesis mother liquor. On the other hand, the molar ratio $\left(\frac{\text{SiO}_2}{\text{Al}_2\text{O}_3}\right)_{\text{FRX molar}} > \left(\frac{\text{SiO}_2}{\text{Al}_2\text{O}_3}\right)_{\text{DRX molar}}$ indicated the difference between global molar and structural molar ratio; the first includes all present phases and the second refers only to zeolitic structure.

Table 1. Chemical composition and specific surface area of the synthesized clay and the zeolite

Solid	SSA (m^2/g)	Chemical composition (FRX)	(Si/Al) _{XRD}
Clay	12	% m SiO_2 = 65,90	-
		% m Al_2O_3 = 13,10	
		$\left(\frac{\text{SiO}_2}{\text{Al}_2\text{O}_3}\right)_{\text{molar}} = 8,55$	
zeolite	376	% m SiO_2 = 34,9	$a_0 = 24,99 \pm 0,01 \text{ \AA}$
		%m Al_2O_3 = 19,7	$\left(\frac{\text{Si}}{\text{Al}}\right)_{\text{XRD}} = 1,08$
		$\left(\frac{\text{SiO}_2}{\text{Al}_2\text{O}_3}\right)_{\text{FRX molar}} = 3,01$	$\left(\frac{\text{SiO}_2}{\text{Al}_2\text{O}_3}\right)_{\text{DRX molar}} = 2,16$

Source: Authors

Characterization of the prepared extrudates (solid adsorbents)

Despite the great industrial importance of producing structured adsorbents and catalysts from powders, few articles directly address structuring. Traditionally, the structuring of catalysts and adsorbents has been developed by companies and maintained as an internal know-how only disclosed in patents (Akthar, Anderson, Ogunwumi, Hedin, and Bergström, 2014).

Single-component clay extrudates and clay-zeolite extrudates were prepared with the synthesized zeolite. Table 2 shows the obtained SSA values. It is worth noting that the extrudates kept their shape after the adsorption experiments.

Table 2. Specific surface area values of extrudates

Solid	Specific surface area (m^2/g)
Extruded clay	10,0
Extruded clay-zeolite	120,0

Source: Authors

The XRD pattern of the extrudates prepared from the PACL-029 clay (Figure 4) is very similar to that of the original clay; only the lines under the 2θ angle are lost. In the XRD pattern of the clay-FAU-Na extrudates, the characteristic lines of the FAU structure are present with a high intensity (Figure 5), indicating that the structure is preserved. They also have all the DRX lines of the clay-only extrudates. The

SSA of the clay extrudates is very similar to the area of the original clay, indicating that the calcination treatment does not appreciably modify the structure of the solid. However, the slight difference in SSA values can be attributed to the lack of heulandite phase in the calcined clay, as indicated by the XRD pattern in Figure 4. The zeolite-clay extrudates reported a higher SSA value due to the contribution of the 40% of zeolite.

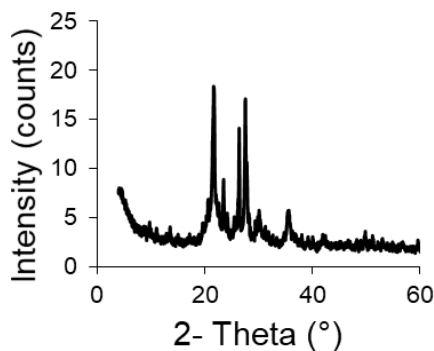


Figure 4. XRD pattern of clay extrudates.

Source: Authors

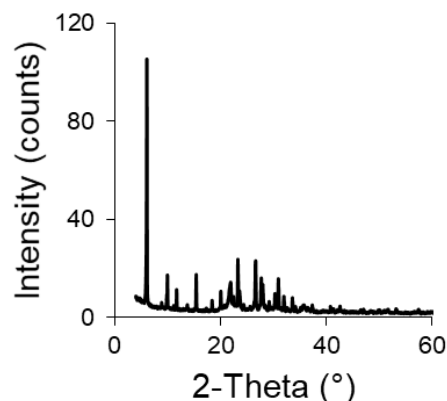


Figure 5. XRD pattern of clay-zeolite extrudates.

Source: Authors

Adsorption studies

Effect of pH on Pb(II) adsorption: With the combined adsorbent zeolite FAU Na-clay PACL-029, the maximum adsorption capacity is obtained at pH 4,97 (Figure 6), in accordance with what was reported by other authors (Pandey et al., 2015; Bai, Wang, and Zhu, 2020; Alsuhybani, Alshahrani, Algamdi, Al-Kahtani, and Alqadami, 2020; Yuan, Xie, Yan, Chen, and Wang, 2018). Figure 7, made with the chemical-equilibrium-diagram tool (Puigdomenech and Of, 2010), illustrates Pb(II) distribution vs pH. The Pb species present vary according to the pH of the solution. Considering only the influence of pH, Pb(II) dominates at low pH, whereas, at neutral-alkaline pH, the precipitation of Pb(OH)₂ is dominant. Pb is amphoteric and, under extreme alkaline conditions (pH > 12), the negatively charged ion Pb(OH)₄²⁻ is dominant (Jensen, Ottosen, and Pedersen, 2006).

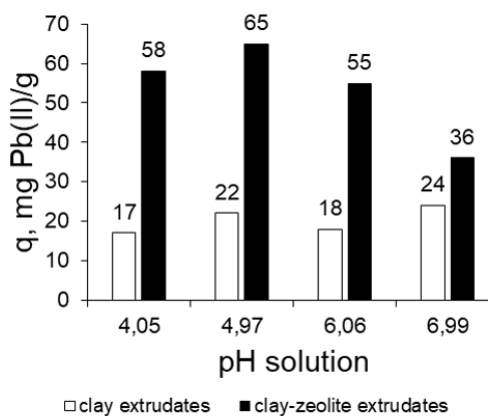


Figure 6. Variation of the adsorption capacity of Pb(II) with changes in pH of the solution.

Source: Authors

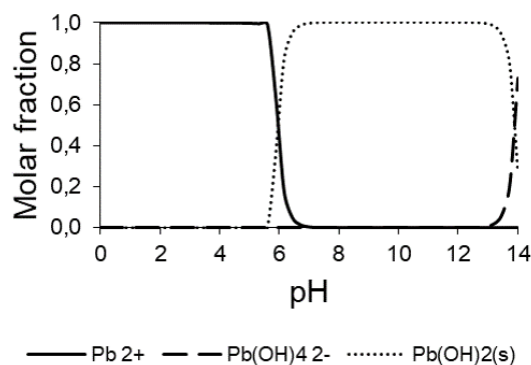


Figure 7. Predominance diagram Pb(II) in solution as a function of pH. Total concentration Pb(II) 80mg/L.

Source: Authors

Pandey *et al.* (2015) found that the removal of Pb(II) increased with increasing pH and recorded its minimum values at 4,0. The above behaviour was explained with the following argument: at lower pH values, the H⁺ ions compete with the metal cation for the adsorption sites on the adsorbent, which in turn leads to partial release of the metal cation. At a higher pH level, the concentration of the H⁺ ions as competing ion decreases, thus resulting in an increase in the amount of removed metal. Additionally, in the zeolite-containing adsorbent, the removal of Pb(II) can be carried out by adsorption and by ion exchange with the exchangeable cations of the zeolite. For a pH close to 5, it is likely that the concentration of interchangeable cations with Pb(II) such as H⁺ and Na⁺ is adequate to increase the adsorption capacity of the solid. With the PACL-029 adsorbent clay, little variation of the adsorption capacity of Pb(II) was obtained in the studied pH interval. In clay, the removal of Pb(II) could occur mainly by adsorption.

Equilibrium isotherm studies: The parameters obtained from isotherm model plots at 30 °C are tabulated in Table 3. Figure 8 shows plots of the linear form of the Langmuir, Freundlich and Temkin isotherm models.

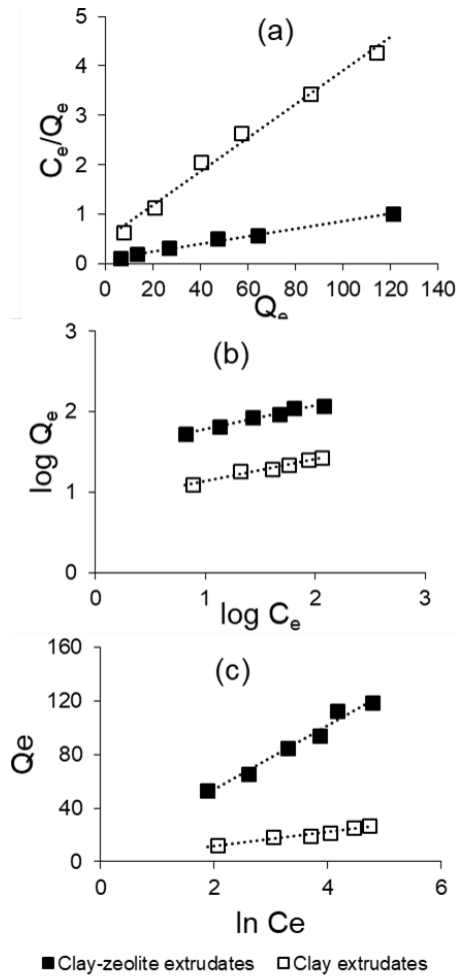


Figure 8. Representation of the isotherm linear forms for the extrudates: (a) Langmuir, (b) Freundlich, (c) Temkin. **Source:** Authors

The best fit was obtained with the Langmuir model. For the determination of the constants of the Langmuir equation, the linear form of the Langmuir model, Equation (1) was employed obtaining acceptable adjustments (Figure 8a). The Langmuir model served to estimate the maximum metal uptake values where they could not be reached by the experiments. The separation factor (R_L) values, calculated through the Langmuir isotherm model for $C_0 = 80$ mg/L (Table 3), indicate that the adsorption is favourable for both adsorbents. The K_L values are comparable, but the maximum adsorption capacity Q_m according to the Langmuir equation is 4 times higher in the combined clay-zeolite extrudate. The representation of the linear Langmuir model in Figure 8a indicates a clear difference between the clay extrudates and the clay-zeolite combination. The zeolitization process remarkably improves the adsorption properties for Pb(II). Clay-zeolite extrudates have a higher adsorption capacity, which may be due to the higher specific surface area value of the extrudates, as well as to a difference in surface composition.

The parameters estimated from the Freundlich plot (Figure 8b) are presented in Table 3. The nature of the adsorptive process can be determined by the value of n (the process

is linear if $n = 1$, chemical if $n < 1$, and physical and favorable if $n > 1$). The values of n are > 1 , which indicates a favorable physisorption condition (Ohale, Onu, Ohale, N., and Oba, 2020).

Table 3. Isotherm parameters of the Langmuir, Freundlich and Temkin models

Langmuir Isotherm				
Extrudates	Qm (mg/g)	K_L (L/mg)	R_L	Linear regression equation
Clay	29,5	0,066	0,098	$\frac{C_e}{Q_e} = 0,034 \left(\frac{1}{C_e}\right) + 0,516$ $R^2 = 0,988$
Clay-zeolite	131,6	0,075	0,053	$\frac{C_e}{Q_e} = 0,0076 \left(\frac{1}{C_e}\right) + 0,101$ $R^2 = 0,994$
Freundlich Isotherm				
Extrudates	K_f (mg/g)	n	Linear regression equation	
Clay	7,23	3,61	$\log Q_e = 0,859 + 0,277 \log C_e$ $R^2 = 0,976$	
Clay-zeolite	31,33	3,45	$\log Q_e = 1,496 + 0,290 \log C_e$ $R^2 = 0,977$	
Temkin Isotherm				
Extrudates	A (L/g)	B	Linear regression equation	
Clay	1,37	5,17	$Q_e = 1,629 + 5,174 \ln C_e$ $R^2 = 0,974$	
Clay-zeolite	1,29	23,90	$Q_e = 6,119 + 23,90 \ln C_e$ $R^2 = 0,973$	

Source: Authors

The parameter B in the Temkin isotherm (Equation 4) is equal to $B = \frac{RT}{b_T}$, where R is the universal gas constant (J/mol K), T is the absolute temperature (K), and b_T (J/mol) is a factor that indicates the adsorbent-adsorbate interaction (Ohale *et al.*, 2020). Then from B , the parameter b_T was determined, obtaining the following values: b_T clay extrudate = 487 J/mol, and b_T clay – zeolite extrudate = 105 J/mol. These indicate a high interaction between adsorbent and the adsorbate, in disagreement with postulates from the Langmuir and Freundlich isotherm models. This model is probably not applicable in the present study. It is worth noting that the fit of the data is not very good.

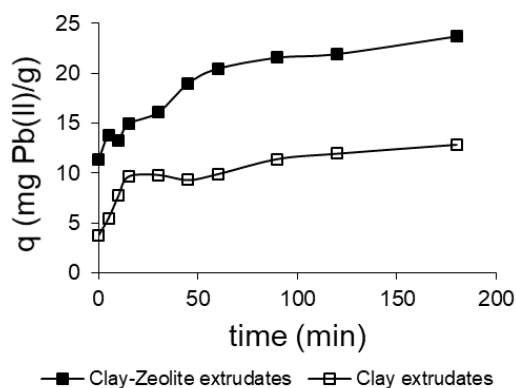
The data from the isotherms, adjusted according to the Langmuir model, indicate that the developed adsorbents are suitable for the adsorption of Pb(II). The maximum adsorption capacity values shown in Table 3 are comparable and even higher than other adsorbents reported in the literature. In Table 4, the maximum adsorption capacity and the adsorption constant according to the Langmuir model are compared for various solid adsorbents reported in previous works.

Adsorption kinetics studies: The kinetic behaviour is an important aspect to study the adsorption process of heavy metal ions in the solid adsorbent. The adsorption capacity q_t for each contact time represented in Figure 9 indicates that the combined adsorbent of the synthesized clay and FAU-Na zeolite has the highest Pb removal capacity.

Table 4. Comparison of the Q_m adsorption capacity and K_L adsorption constant of the Langmuir model with different solid adsorbents

Adsorbent	Q_m (mg/g)	K_L L/mg	Reference
Zeolite Na-X synthetic Si/Al = 1,37	14,22	0,0976	(Pandey <i>et al.</i> , 2015)
nFe@ZIF-8 (Zeolitic Imidazole Framework-8 modified with Fe)	182,0	2,87	(Zhou <i>et al.</i> , 2020)
ZCET-40 (material obtained from coal ash containing the zeolites NaP1, Hidroxisodalite and Analcima)	88,0	0,0002	(Visa, 2016)
Activated carbon with Fe	52,0	0,15	(Liu, Lai, and Wang, 2019)
FA24 adsorbent (synthesized from ashes consisting mainly of Hydroxisodalite)	38-40,5	0,11-0,16	(Kobayashi <i>et al.</i> , 2020)
Composite material Polyacrylonitrile/zeolite NaY, functionalized with Hydroxylamine	73,35	0,9015	(Elwakeel <i>et al.</i> , 2018)

Source: Authors


Figure 9. Adsorption capacity as a function of contact time for the two prepared adsorbents.

Source: Authors

The complete course of adsorption includes mass transfer and comprises three steps: (i) film diffusion (external diffusion), which is the transport of adsorptive from the bulk phase to the external surface of the adsorbent; (ii) pore diffusion (intra-particle diffusion), which is the transport of adsorptive from the external surface into the pores; and (iii) surface reaction, which is the attachment of adsorptive to the internal surface of sorbent (Tan and Hameed, 2017).

The surface reaction kinetics were studied with the pseudo first order, pseudo second order, and Elovich models stated in Equations (7), (8), and (9), respectively. Table 5 shows the parameters estimated from the plots of these models as described earlier in Experimentation section.

The graphs corresponding to the linear Equations (7), (8), and (9) are shown in Figure 10. The best fit was obtained by the second-order model. The q_e values obtained from pseudo first order and Elovich models were different from the actual q_e values obtained experimentally (Table 5). This suggests that these models were unsuitable to describe the adsorptive rate

processes. However, q_e values of the pseudo second order model showed good agreement with experimental q_e values. The evaluated regression coefficients were satisfactorily high ($R^2 \sim 0,99$) for the PSO model than for other sorption models.

Table 5. Adsorption kinetic parameters obtained by the PFO, PSO, and Elovich models

Pseudo first order model (PFO)			
Extrudates	$q_e \frac{mg Pb(II)}{g}$	$k_1 \text{ min}^{-1}$	Linear regression equation
Clay	6,55	0,0165	$\ln(q_e - q) = 1,880 - 0,0165 t$ $R^2 = 0,882$
Clay-Zeolite	11,35	0,0172	$\ln(q_e - q) = 2,429 - 0,0172 t$ $R^2 = 0,9655$
Pseudo second order model (PSO)			
Extrudates	$q_e \frac{mg Pb(II)}{g}$	$k_2 \left(\frac{g}{min \cdot mg Pb(II)} \right)$	Linear regression equation
Clay	12,94	0,0088	$\frac{t}{Q_t} = 0,6742 + 0,0773 t$ $R^2 = 0,989$
Clay-Zeolite	24,04	0,0055	$\frac{t}{Q_t} = 0,3434 + 0,0416 t$ $R^2 = 0,994$
Elovich model			
Extrudates	$\alpha \frac{mg Pb(II)}{g \text{ min}}$	β	Linear regression equation
Clay	3,16	0,466	$q = 1,061 + 2,143 \ln t$ $R^2 = 0,9201$
Clay-Zeolite	18,49	0,317	$q = 5,580 + 3,153 \ln t$ $R^2 = 0,9372$

Source: Authors

The values of the adsorption rate constant (k_2) are of the same order in the clay extrudates and in the combined extrudate, and the latter has twice the adsorption capacity. The pseudo second order kinetic model has been reported in several investigations on Pb(II) removal in aqueous systems. Table 6 shows the kinetic parameter values reported in other investigations. Like the data indicated by the adjustment with the Langmuir isotherm model, these data indicate that the two prepared adsorbents are suitable for the Pb(II) removal.

To determine whether pore diffusion was the only rate-limiting step in the adsorptive study of this system, experimentally obtained kinetic data was fitted to the Bangham-Burt model stated in Equation (10). The linear plot presented in Figure 11b and the corresponding R^2 values given in Table 7 suggest that pore and film diffusion influenced the kinetic mechanism.

The Webber-Morris intraparticle diffusion model (Equation 11) was used to examine the contributions of each diffusion step in the overall mass transfer mechanism: external and intra-particle (Robati, 2013; Chu *et al.*, 2019). Results of model plot are presented in Figure 11a. This Figure shows two linear segments, which implies that adsorptive mass transfer took place under two steps. The first segment signifies an external

surface adsorption associated with liquid film diffusion, while the second segment depicts an adsorption controlled by intra-particle diffusion. The intra-particle diffusion rate constant (k_{id1} and k_{id2}) estimated from both segments is presented in Table 7.

Table 6. Comparison of the kinetic parameters of the pseudo second order model reported in previous investigations

Solid adsorbent	$q_e \frac{mg Pb(II)}{g}$	$k_2 \left(\frac{g}{min \cdot mg Pb(II)} \right)$	Reference
Graphene oxide / alginate hydrogel membrane	163,0	0,324	(Bai et al., 2020)
Magnetic nanoparticles covered with benzoic acid functionalized with aminoguanidinopentanoic acid	19,53	0,0017	(Alshybiani et al., 2020)
HCTMABr Modified Micronized Clinoptilolite	0,304	0,6536	(Shirzadi and Nezamzadeh-Ejehieh, 2017)
Zeolite USY with alkaline treatment	4,03	0,1070	(Sulaiman et al., 2020)
Clinoptilolite-glycine	4,14	0,032	(Nasiri-Ardali and Nezamzadeh-Ejehieh, 2020)

Source: Authors

Table 7. Parameters obtained from intra-particle diffusion kinetic models

Webber-Morris' model			
Extrudates	$k_{id} \frac{mg}{g \cdot min^{1/2}}$	$B \frac{mg}{g}$	Linear regression equation
Clay	$k_{id1} = 1,23$	$B_1 = 3,64$	$q_1 = 3,64 + 1,23t^{1/2} R^2 = 0,9017$
	$k_{id2} = 0,54$	$B_2 = 5,87$	$q_1 = 5,87 + 0,54t^{1/2} R^2 = 0,9615$
Clay-Zeolite	$k_{id1} = 11,39$	$B_1 = 0,84$	$q_1 = 11,69 + 0,85t^{1/2} R^2 = 0,927$
	$k_{id2} = 15,06$	$B_2 = 0,65$	$q_2 = 15,06 + 0,65t^{1/2} R^2 = 0,9582$

Bangham's model			
Extrudates	k_0	α	Linear regression equation
Clay	18,30	0,31	$\log \left(\log \left(\frac{C_0}{C_0 - q_m} \right) \right) = -1,80 + 0,31 \log t$ $R^2 = 0,8667$
Clay-Zeolite	53,22	0,22	$\log \left(\log \left(\frac{C_0}{C_0 - q_m} \right) \right) = -1,34 + 0,22 \log t$ $R^2 = 0,8667$

Source: Authors

Conclusions

Zeolite X with Si/Al = 1,08 ratio was synthesized from clay, using synthesis mixture compositions employed in synthesis from aluminosilicate gels. The characterization carried out indicated adequate properties in the synthesized zeolite, such as purity, crystallinity, and specific area. The zeolite in the

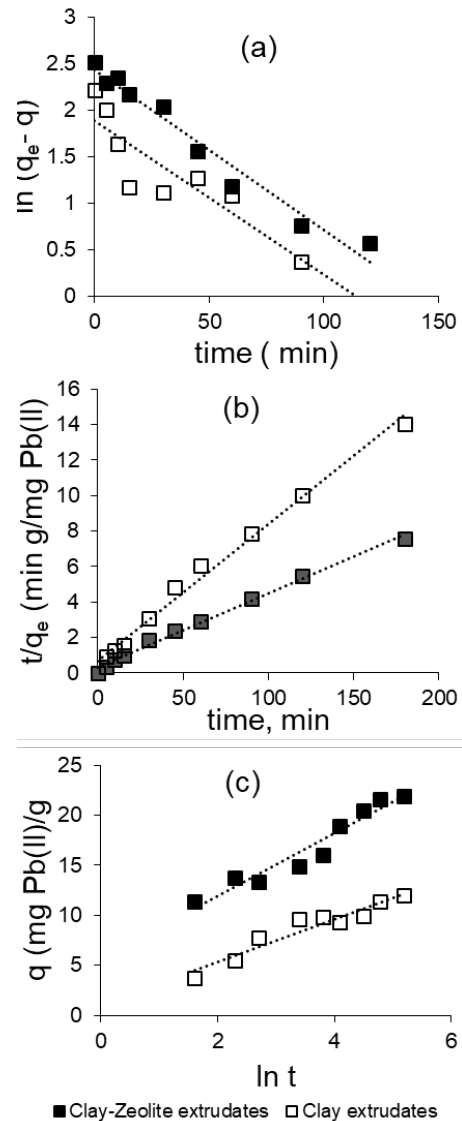


Figure 10. Kinetic plots for (a) Pseudo first order model, (b) Pseudo second order model and (c) Elovich model.

Source: Authors

extrudate maintains the crystalline structure and increases the specific surface area 10 times compared to the clay-only material, notably improving the adsorption capacity of Pb(II), which is favoured at pH = 5. The adsorption equilibrium isotherm (at 30 °C) was adjusted applying the Langmuir model, with a separation factor R_L indicating favorable adsorption. The maximum adsorption capacity Q_m was 132 mg Pb(II)/g, a comparable value and even higher than reported values for a variety of solid adsorbents. The adsorption kinetics were adjusted to the pseudo second order model with chemical adsorption controlling the process. The value of the kinetic constant is of the same order in the evaluated materials. However, in the combined material, the adsorption capacity q_e is almost double. The liquid film diffusion and intra-particle diffusion influence the kinetic mechanism.

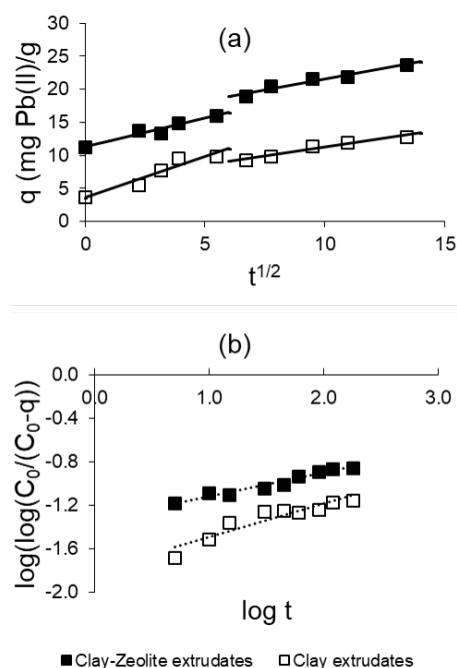


Figure 11. Kinetic plots for (a) Webber Morris model (b) Bangham model.

Source: Authors

Acknowledgements

The authors acknowledge the Master's degree program in Applied Chemistry of Universidad Técnica Particular de Loja for funding this research, as well as Dr. Paulina Aguirre and Mgtr. Diego Maza for their collaboration in the adsorption experiments.

References

- Ahrouch, M., Gatica, J., Draoui, K., Bellido, D., and Vidal, H. (2019). Lead removal from aqueous solution by means of natural clays honeycomb monoliths. *Journal of Hazardous Materials*, 365, 519-530. 10.1016/j.jhazmat.2018.11.037
- Akthar, F., Anderson, L., Ogunwumi, S., Hedin, N., and Bergström, L. (2014). Structuring adsorbents and catalyst by processing of porous powders. *Journal of the European Ceramic Society*, 34(7), 1643-1666. 10.1016/j.jeurceramsoc.2014.01.008
- Albis, A., Martínez, J., Severiche, M., and García, J. (2016). Removal of lead from aqueous solution using cassava peel modified with citric acid. *Avances: Investigación en Ingeniería*, 13(1), 1-11. 10.18041/1794-4953/avances.2.254
- Alsuhybani, M., Alshahrani, A., Algamdi, M., Al-Kahtani, A., and Alqadami, A. (2020). Highly efficient removal of Pb(II) from aqueous systems using a new nanocomposite: Adsorption, isotherm, kinetic and mechanism studies. *Journal of Molecular Liquids*, 301, 112393. 10.1016/j.molliq.2019.112393
- Gilson Co. (n.d.) *ASTM test sieves*. <https://www.globalgilson.com/astm-test-sieves>
- Ayele, L., Pérez-Pariente, J., Chebude, Y., and Díaz, I. (2016). Conventional versus alkaline fusion synthesis of zeolite A from low grade kaolin. *Applied Clay Science*, 132-133, 485-490. 10.1016/j.clay.2016.07.019
- Bai, S., Zha, L., Chang, Z., Zhang, Ch., and Chu, M. (2018). Synthesis of Na-X zeolite from Longkou oil shale ash by alkaline fusion hydrothermal method. *Carbon Resources Conversion*, 1(3), 245-250. 10.1016/j.crcon.2018.08.005
- Bai, Ch., Wang, L., and Zhu, Z. (2020). Adsorption of Cr(III) and Pb(II) by graphene oxide/alginate hydrogel membrane: Characterization, adsorption kinetics, isotherm and thermodynamics studies. *International Journal of Biological Macromolecules*, 147, 898-910. 10.1016/j.ijbiomac.2019.09.249
- Belova T., (2019). Adsorption of heavy metal ions (Cu+2, Ni+2, Co+2 and Fe+2) from aqueous solutions by natural zeolite. *Heliyon*, 5(9), e02320. 10.1016/j.heliyon.2019.e02320
- Bhatt, A., Sakaria, P., Vasudeven, M., Pawar, R., Sudheesh, N., Bajaj, H., and Mody, H. (2012). Adsorption of an anionic dye from aqueous medium by organoclays: equilibrium modeling, kinetic and thermodynamic exploration. *RSC Advances*, 2(23) 8663-8671. 10.1039/C2RA20347B
- Boskabady, M., Marefati, N., Farkhondeh, T., Shakeri, F., Farshbaf, A., and Boskabady, H. M. (2018). The effect of environmental lead exposure on human health and the contribution of inflammatory mechanisms, a review. *Environment International*, 120, 404-420. 10.1016/j.envint.2018.08.013
- Boycheva, S., Marinov, I., Miteva, S., and Zgureva, D. (2020). Conversion of coal fly ash into nanozeolite Na-X by applying ultrasound assisted hydrothermal alkaline activation. *Sustainable Chemistry and Pharmacy*, 15, 100217. 10.1016/j.scp.2020.100217
- Bustillo, M., Fort, R., and Bustillo, M. (1993). Specific surface area and ultramicroporosity in polymorphs of silica. *European Journal of Mineralogy*, 5(6) 1195-1204. 10.1127/ejm/5/6/1195
- Carolin, F. C., Kumar, S. P., Saravanan, A., Joshiba J. G., and Naushad, M. (2017). Efficient techniques for the removal of toxic heavy metals from aquatic environment: A review. *Journal of Environmental Chemical Engineering*, 5(3), 2782-2799. 10.1016/j.jece.2017.05.029
- Chu, Y., Khan, M., Wang, F., Xia, M., Lei, W., and Zhu, S. (2019). Kinetics and equilibrium isotherms of adsorption of Pb(II) and Cu(II) onto raw and arginine-modified montmorillonite. *Advance Powder Technology*, 30(5), 1067-1078. 10.1016/j.apt.2019.03.002
- Elwakeel, K., El-Bindary, E., Kouta, E., and Guibal, E. (2018). Functionalization of polyacrylonitrile/Na-Y-zeolite composite amidoxime groups for the sorption of Cu(II), Cd(II) and Pb(II) metal ions. *Chemical Engineering Journal*, 332, 727-736. 10.1016/j.cej.2017.09.091
- García, A., López, C. M., García, L., Casanova, J., and Goldwasser, M. (2016). Improvements in the synthesis with low Si/Al

- ratio from Venezuelan sodium silicate for an environmentally friendly process. *Ingeniería e Investigación*, 36(1), 62-69. 10.15446/ing.investig.v36n1.52855
- Giannetto, G., Montes, A., and Rodríguez, G. (2000). *Zeolitas: Características, propiedades y aplicaciones industriales*. Caracas, Venezuela: Innovación Tecnológica, Universidad Central de Venezuela.
- Inyibor, A., Adekola, F., and Olatunji, G. (2016). Kinetics, isotherms and thermodynamic of liquid phase adsorption of Rhodamine B dye onto Raphia hookerie fruit epicarp. *Water Resources and Industry*, 15, 14-27. 10.1016/j.wri.2016.06.001
- Jensen, P., Ottosen, L., and Pedersen, J. (2006). Speciation of Pb in industrially polluted soils. *Water, Air, and Soils Pollution*, 170, 359-382. 10.1007/s11270-005-9008-7
- Ke, G., Shen, H., and Yang, P. (2019). Synthesis of X-zeolite from waste basalt powder and its influencing factors and synthesis mechanism. *Materials*, 12(23), 3895. 10.3390/ma12233895
- Kobayashi, Y., Ogata, F., Nakamura, T., and Kawasaki, N. (2020). Synthesis of novel zeolites produced from fly ash by hydrothermal treatment in alkaline solution and its evaluation as an adsorbent for heavy metal removal. *Journal of Environmental Chemical Engineering*, 8(2), 103687. 10.1016/j.jece.2020.103687
- Kongnoo, A., Tontisirin, S., Worathanakul, P., and Phalakornkule, Ch. (2017). Surface characteristics and CO₂ adsorption capacities of acid-activated zeolite 13X prepared from palm oil mill fly ash. *Fuel*, 193, 385-394. 10.1016/j.fuel.2016.12.087
- Liu, X., Lai, D., and Wang, Y. (2019). Performance of Pb(II) removal by an activated carbon supported nanoscale zero-valent iron composite at ultralow iron content. *Journal of Hazardous Materials*, 361, 37-48. 10.1016/j.jhazmat.2018.08.082
- Luo, H., Lau, W., Wu, Y., Zhu, W., and Yang, E-H. (2018). Hydrothermal synthesis of needle-like nanocrystalline zeolites from metakaolin and their applications for efficient removal of organic pollutants and heavy metals. *Microporous Mesoporous Materials*, 272, 8-15. 10.1016/j.micromeso.2018.06.015
- Montalvo, S., Huiliñir, C., Borja, R., Sánchez, E., and Hermann, C. (2020). Applications of zeolites for biological treatment processes of solids wastes and wastewaters – A review. *Bioresource Technology*, 301, 122808. 10.1016/j.biortech.2020.122808
- Moussi, B., Hajjaji, W., Hachani, M., Hatira, N., Labruncha, J., Yans, J., and Jamoussi, F. (2020). Numidian clay deposits as raw material for ceramics tile manufacturing. *Journal of African Earth Science*, 164, 103775. 10.1016/j.jafrearsci.2020.103775
- Nasiri-Ardali, M., and Nezamzadeh-Ejhieh, A. (2020). A comprehensive study on the kinetics and thermodynamic aspects of batch and column removal of Pb(II) by the clinoptilolite-glycine adsorbent. *Materials Chemistry Physics*, 240, 122142. 10.1016/j.matchemphys.2019.122142
- Ohale, P., Onu, C., Ohale, N., and Oba, S. (2020). Adsorptive kinetics, isotherm and thermodynamic analysis of fishpond effluent coagulation using waste Brachyura shell. *Chemical Engineering Journal Advances*, 4, 100036. 10.1016/j.cej.2020.100036
- Pandey, P., Sharma, S. K., and Sambhi, S. (2015). Removal of lead(II) from waste water on zeolite NaX. *Journal of Environmental Chemical Engineering*, 3(4), 2604-2610. 10.1016/j.jece.2015.09.008
- Poma, P. (2008). Intoxicación por plomo en humanos. *Anales de la Facultad de Medicina*, 69(2), 120-126.
- Puigdomenech, I. and Of, K. R. I. T. (2010). *MEDUSA, HYDRA and INPUT-SED-PREDOM*. <https://www.kth.se/che/medusa/>
- Ramola, S., Belwal, T., Li, C., Wang, Y., and Zhou, Ch. (2020). Improved lead removal from aqueous solution using novel porous bentonite and calcite biochar composite. *Science of the Total Environment*, 709, 136171. 10.1016/j.scitotenv.2019.136171
- Robati, D. (2013). Pseudo second order kinetic equations for modeling adsorption systems for removal of lead ions using multi walled carbon nanotube. *Journal of Nanostructure in Chemistry*, 3(1), 55. 10.1186/2193-8865-3-55
- Shariatina, Z. and Bagherpour, A. (2018). Synthesis of zeolite NaY and its nanocomposite with chitosan adsorbents for lead(II) removal from aqueous solution. *Powder Technology*, 338, 744-763. 10.1016/j.powtec.2018.07.082
- Shirzadi, H. and Nezamzadeh-Ejhieh, A. (2017). An efficient modified zeolite for simultaneous removal of Pb(II) and Hg(II) from aqueous solution. *Journal of Molecular Liquids*, 230, 221-229. 10.1016/j.molliq.2017.01.029
- Sulaiman, K., Sajid, M., and Alhooshani, K. (2020). Application of porous membrane bag enclosed alkaline treated Y-zeolite for removal of heavy metal ions from water. *Microchemical Journal*, 152, 104289. 10.1016/j.microc.2019.104289
- Tan, K. and Hameed, B. (2017). Insight into the adsorption kinetics models for the removal of contaminants from aqueous solutions. *Journal of the Taiwan Institute of Chemical Engineers*, 74, 25-48. 10.1016/j.jtice.2017.01.024
- Tracy, J. and Higgins, B. (2001). *Collection of Simulated XRD Powder Patterns for Zeolites*. Structure Commission of the International Zeolite Association.
- Uddin, K. M. (2017). A review on the adsorption of heavy metals by clay minerals, with special focus on the past decade. *Chemical Engineering Journal*, 308, 438-462. <https://doi.org/10.1016/j.cej.2016.09.029>
- Visa, M., (2016). Synthesis and characterization of new zeolites obtained from fly ash for heavy metals removal in advanced wastewater treatment. *Powder Technology*, 294, 338-347. 10.1016/j.powtec.2016.02.019
- Wajima, T. and Ikaezami, Y. (2009). Synthesis of crystalline zeolite 13X from waste porcelain using alkali fusion. *Ceramics International*, 35(7), 2983-2986. 10.1016/j.ceramint.2009.03.014

- Wang, H., Zhou, A., Peng, F., Yu, H., and Yang, J. (2007). Mechanism study on adsorption multiwalled carbon nanotubes. *Journal of Colloid Interface Science*, 316(2) 277-283. 10.1016/j.jcis.2007.07.075
- Wi, S., Yang, S., Park, J., Chang, S., and Kim, S. (2020). Climatic cycling assessment of red clay/perlite and vermiculite composite PCM for improving thermal inertia in building. *Building Environmental*, 167, 106464. 10.1016/j.buildenv.2019.106464
- Webb, P., Orr, C., Camp, R., Olivier, J., and Yunes, S. (1997). *Analytical methods in fine particle technology*. Norcross, GA: Micromeritics Instrument Corporation.
- Yuan, M., Xie, T., Yan, G., Chen, Q., and Wang, L. (2018). Effective removal of Pb+2 from aqueous solutions by magnetically modified zeolite. *Powder Technology*, 332, 234-241. 10.1016/j.powtec.2018.03.043
- Zafarzadeh, A., Sadeghi, M., Golbini-Mofrad, A., and Beirami, S. (2018). Removal of lead by activated carbon and citrus coal from drinking water. *Desalination Water Treatment*, 105, 282-286. 10.5004/dwt.2018.22024
- Zhou, L., Li, N., Jin, X., Owens, G., and Chen, Z. (2020). A new nFe@ZIF-8 for the removal of Pb(II) from wastewater by selective adsorption and reduction. *Journal of Colloid Interface Science*, 565, 167-176. 10.1016/j.jcis.2020.01.014